Influence of Solidification-Dependent Microstructure on Subsequent Metal Forming Operations

Johannes Kronsteiner[1], Sindre Hovden[1], Stephan Jäger[1], Evgeniya Kabliman[2]

[1]LKR Light Metals Technologies, Austrian Institute of Technology, Giefinggasse 2, 1210 Vienna, Austria
[2]Technical University of Munich, TUM School of Engineering and Design, Department of Mechanical Engineering, Chair of Materials Engineering of Additive Manufacturing, Boltzmannstr. 15, 85748 Garching, Germany

Abstract

Conventional metal deformation simulations which include microstructure evolution would not consider any initial spatial variations but assume a uniform microstructure. In metal manufacturing, the liquid phase during casting and its subsequent solidification play major roles in characterizing the material properties (both micro- and macroscopic). Physics-based material models allow to simulate microstructural effects based on measurable microstructural properties. However, some parameters such as the grain size vary considerably within the manufactured part geometry depending on the processing conditions. Since the grain size distribution influences the microstructure evolution during subsequent heat treatment (HT) and metal forming operations, considering a more realistic initial distribution can be beneficial for subsequent simulations.
In the proposed workflow, a simulation of grain growth during solidification generates the initial spatial information ensuring the accuracy of following metal deformation simulations. The resulting microstructure (grain size distribution) is afterwards mapped onto the following deformation and HT process simulations. The results are demonstrated for a lab-scale hot compression test. By comparison with a homogeneous initial grain size distribution, the influence of heterogeneity on the materials static recrystallization behavior after the deformation was investigated. The performed study opens the opportunity for further investigations of more complex geometries for industrial applications (e.g. extrusion, rolling etc.).

1 Introduction

To optimize the properties of high performance materials in automotive and aerospace industries, the process conditions during the whole processing chain from casting to metal forming operations are of utmost importance. Each process has a distinct influence on the microstructure and thus on the material properties of the final component. As a result, scientists and engineers started to incorporate the influence of microstructural changes into physics-based material models. In the studies [1-3], the material behavior during metal forming operations was described by the evolution of microstructural properties. The evolution of the grain diameter was modelled in [1] based on the Avrami equation. It was possible to describe the relationship between recrystallized volume fraction and effective strain. In [2-4], the simulation of hot rolling with subsequent heat treatment (HT) process was realized by using a model based on the evolution of dislocation density and later named: “Mean Dislocation Density based Material” (MD^{2}M) model.
The MD^{2}M model operates with microstructural properties, such as grain size distribution, which are often not evenly distributed due to the complex boundary conditions of the production processes. In the case of casting, the heterogeneous grain size distribution after solidification has an impact on the microstructural evolution during subsequent HT and forming processes. However, the general approach for the simulation of metal forming processes, even when considering microstructure evolution, is to start from a uniform or random distribution.
The aim of the present work is to improve the prediction of microstructure evolution during metal forming and HT processes by using the heterogeneous initial grain diameter distribution after solidification as initial conditions for the subsequent process simulations. The whole presented simulation sequence is an elaborate example of a *Through Process Simulation* (TPS) approach.

2 Methods

To assess the impact of considering a heterogeneous grain size distribution after solidification on the recrystallization behavior, the following approach was designed;
For the simulation of grain growth during solidification, a Cellular Automaton (CA) algorithm was used. The resulting spatial grain size distribution was afterwards mapped from the CA lattice onto the LS-DYNA® mesh for metal forming and heat treatment (HT) simulations. The mapping between the different meshes (very fine CA lattice to comparably coarse FEM mesh) was performed by using the preCICE [5] coupling library. Afterwards, the HT and forming processes were simulated coupled with precipitation kinetics calculations. For demonstration purposes, a cylindrical sample made of AA2024 was used for a lab-scale uniaxial hot compression test. A number of alloy elements were reduced to a binary Al-Cu system in the grain growth simulations, while a conventional composition of AA2024 was used for the FEM and precipitation kinetics simulations. The latter were performed using a CALPHAD-based approach implemented into the commercial software MatCalc.
The simulated process chain was the following and is depicted in Fig. 1:

- Solidification simulation using CA.
- HT simulation considering precipitation kinetics.
- Compression at constant temperature and strain rate.
- Post-HT.

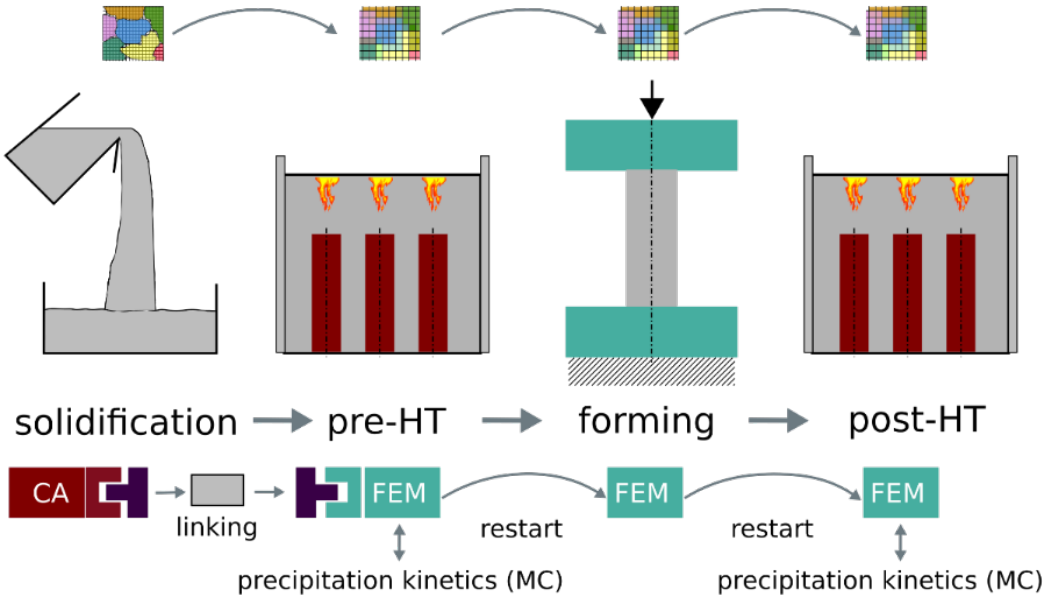

Fig.1: Process chain considered for the demonstration of the Through Process Simulation (TPS) concept.

2.1 Grain growth simulation using LB-CA

The grain growth during solidification was simulated by implementing a CA algorithm [6] into the lattice Boltzmann Method (LBM) based solver palabos [7]. The aim of the grain growth simulation was to provide a realistic heterogeneous grain size distribution for mapping. In order to keep the computational effort acceptable, some simplifications regarding the physics were made:

(1) fluid flow (forced and natural convection) was neglected;
(2) latent heat was neglected;
(3) no solutal segregation (spatially homogeneous solute concentration) was assumed;
(4) grain growth was driven by thermal undercooling;
(5) grains were approximated as spherical after mapping to FEM.

The heat equation was solved by LBM for the temperature *T* and thermal diffusivity α using Eq. (1):

$$\frac{\partial T}{\partial t} - \alpha \nabla^2 T = 0 \quad (1)$$

The temperature field from LBM was transferred to the grain growth model implemented into CA by a unidirectional interface. The assumption of thermal undercooling driven grain growth ensures the applicability of the Kurz, Giovanola, Trivedi (KGT) grain growth model [8].

2.2 Thermo-kinetic simulations

To obtain the necessary input for the flow stress and recrystallization models, the local microchemistry was simulated during HT processes using MatCalc [9]. To study the precipitation kinetics, the following series of thermo-kinetic simulations (see Fig. 1) was carried out. At first: (1) the Scheil-Gulliver [10-11] equation is applied to calculate the distribution of primary precipitates in addition to the LB-CA solidification simulation; (2) the artificial HT step (similar to a homogenization) was simulated to obtain the phase distribution for the non-deformed samples; (3) initial distributions (particle size/density/fraction) of the non-deformed samples for the forming simulations were obtained; (4) simulation of the post-heating steps (see Fig. 1). All HT simulations were performed by coupling thermal/precipitation calculations using LS-DYNA® and MatCalc.

2.3 Flow stress model

The MD²M model was implemented into the general-purpose Finite Element (FEM) solver LS-DYNA® to describe the materials behavior during the deformation (flow stress) and sub-sequent heat treatment (static recrystallization). This model is using material internal variables, e.g. a dislocation density, and depends on strain, strain rate and temperature. The flow stress is described by using a Kocks-Mecking approach [12, 13] by a superposition of production and annihilation of mean dislocation density [2-4]. The dislocation density increases during material deformation and decreases during recovery and recrystallization processes. The change of mean dislocation density, ρ, from time step $^{t-1}$ to ^{t} is described by Eq. (2). The parameters for Eqs. (2-11) and corresponding values used for all simulations are summarized in Tab. 1.

$$\frac{\partial \rho^t}{\partial t} = \frac{M\sqrt{\rho^{t-1}}}{b \cdot A}\dot{\varphi} - 2 \cdot B\,\frac{d_{ann}}{b}\rho^{t-1} \cdot \dot{\varphi} \cdot M - 2 \cdot C \cdot D_s(T)\,\frac{G(T) \cdot b^3}{k_B \cdot T}\left[(\rho^{t-1})^2 - \left(\rho_{eq}\right)^2\right] \tag{2}$$

The sub-grain boundary energy γ_{sub} is calculated during the forming process by:

$$\gamma_{sub}^t = \gamma_{sub}^{t-1} + \frac{0.8}{2 \cdot \sqrt{\rho_g^t}} \cdot G(T) \cdot b^2 \cdot \frac{K}{3} \cdot d\rho_g^{t-1}. \tag{3}$$

The evolution of sub-grain size δ during forming operations is calculated by

$$\delta^t = \delta^{t-1} - \frac{(\delta^{t-1})^3}{2 \cdot K^2}. \tag{4}$$

The flow stress σ at the current time step t based on the dislocation density is calculated by

$$\sigma^t = M \cdot G(T)\left[0.5 \cdot \sqrt{\rho^{t-1}} + \left(\frac{1}{\delta^{t-1}}\right)\right]. \tag{5}$$

To fit the alloy-dependent forming behavior, the alloy specific physical properties as well as three fitting parameters (A, B, C) need to be adapted [14]. The values of (A, B, C) are temperature and strain rate dependent parameters and were determined by fitting the calculated flow stress to the results of compression tests performed by a quenching dilatometer DIL805A/D from TA instruments. Before fitting the model parameters, the measured flow stress curves were temperature compensated based on [15] using an in-house developed code.

The equations describing the flow stress were implemented as an elasto-viscoplastic material model into a user-defined material subroutine (UMAT47v) of LS-DYNA®.

2.4 Static recrystallization model

The static recrystallization part of the MD²M model was implemented into the thermal user-defined material model (THUMAT11) in LS-DYNA®. This model uses the results from the deformation step, e.g. final values of dislocation density and sub-grain boundary energy and solves the following equations; The retarding force $P_{Z,sub}$ is calculated by:

$$P_{Z,sub} = 2 \cdot \pi \cdot \gamma_{sub}^t \cdot N_{part} \cdot r_{part}^2, \tag{6}$$

where N_{part} and r_{part} are number density and mean radius of nano-size particles, correspondingly, calculated using MatCalc. The driving force P_D is calculated considering ρ, γ_{sub} and δ by:

$$P_D = \frac{1}{2}G(T) \cdot b^2 \cdot \left(\rho^t - \rho_{eq}\right) - \left(\frac{3 \cdot \gamma_{sub}^t}{\delta^t}\right). \tag{7}$$

Subgrain diameter (δ) is calculated for time t by:

$$\frac{d\delta^t}{dt} = M \cdot \left(\frac{3 \cdot \gamma_{sub}}{\delta^{t-1}} - \frac{3 \cdot \gamma_{sub}}{\delta_{eq}} - P_{Z,sub}\right). \tag{8}$$

The recrystallized grain diameter d_{REX}^t can be then calculated using P_D and $P_{Z,sub}$ by:

$$\frac{\mathrm{d}d_{rex}^t}{\mathrm{d}t} = M \cdot \left(P_D^{t-1} - P_{Z,sub}\right) \cdot (1 - X_{SRX}^{t-1}). \tag{9}$$

The recrystallized grain fraction X^t is calculated by:

$$X_{SRX}^t = X_{SRX}^{t-1} + \frac{\pi}{6}\left[\Delta N \cdot (d_{REX}^{t-1})^3 + 3 \cdot N^{t-1} \cdot (d_{REX}^{t-1})^2 \cdot \frac{\mathrm{d}d_{REX}^t}{\mathrm{d}t}\right]. \quad (10)$$

Finally, the average grain diameter is calculated using:

$$d^t = d^{t-1} \cdot (1 - X^{t-1}) + d_{REX}^{t-1} \cdot X^{t-1}, \quad (11)$$

Description	Parameter	Value	Units
Time	t		[s]
Taylor factor for random (fcc) textures	M	3.06	[-]
Length of the Burger's vector	b	2.86e-10	[m]
Alloy specific fitting parameters	A, B, C, K	11.0,60.0,1.0e-4,12.0	[-]
Local strain rate	$\dot{\varphi}$	calculated	[s^{-1}]
Critical distance for spontaneous annihilation	$d_{ann}(T)$	calculated: ~2.89e-10	[m]
Mean, equilibrium dislocation density	ρ, ρ_{eq}	calculated, 1.0e11	[m^{-2}]
Auxiliary dislocation density	ρ_g	calculated	[m^{-2}]
Diffusion coefficient in solid state	D_s(T)	calculated: ~3.03e-11	[m^2s^{-1}]
Temperature dependent shear modulus	$G(T)$	calculated: ~2.055e10	[Nm^{-2}]
Boltzmann constant	k_B	1.381e-23	[J/K]
Temperature	T	calculated	[K]
Subgrain boundary energy	γ_{sub}	calculated	[Jm^{-2}]
Subgrain size, equilibrium subgrain size	δ, δ_{eq}	calculated, 3.795e-5	[m]
Flow stress	σ	calculated	[Nm^{-2}]
Retarding force (Zener drag)	$P_{Z,sub}(N_{part}, r_{part}, \chi)$	calculated	[J]
Number of nano-sized particles	N_{part}	calculated: ~1.0e19	[-]
Radius of nano-sized particles	r_{part}	calculated: ~1.0e-8	[m]
Grain diameter	d	calculated	[m]
Recrystallized grain diameter	d_{REX}	calculated	[m]
Statically recrystallized grain fraction	X_{SRX}	calculated	[-]
Driving force (stored energy)	$P_D(T, \rho, \delta, \gamma_{sub})$	calculated	[J]
Number of nucleii	$N(X_{SRX})$	calculated	[-]
Change of number of nucleii	ΔN	calculated	[-]

Table 1: Parameters of Eqs. (2) - (11).

2.5 Data mapping from grain growth simulation to forming simulation

The grain diameters d_I (where I is the grain number) and the corresponding volumetric centers $\overrightarrow{G_I}$ from the grain growth simulation were mapped to the forming simulation. For this purpose, the coupling library preCICE was used [5]. Although preCICE can be applied for the coupling of multiple solvers during run time, here, a one-shot mapping without any progress in time was used. preCICE is able to map any data (scalar, vector) between point clouds. In the presented case, one point cloud was provided by the grain growth simulation and one by the forming simulation. The coordinates provided by the grain growth simulation were calculated as the grains' volumetric centers. The destination coordinates in the forming simulation were determined as the volumetric centers of the finite elements. The global mapping from the grain point cloud $\overrightarrow{G_I}$ to the finite element point cloud $\overrightarrow{F_I}$ was determined using radial basis functions as explained in [16] with the compact polynomial "c0" [5]. The cut-off radius was chosen in the order of 2 to 3 times the maximum element edge length of the finite element forming mesh.

3 Show case: compression test

To demonstrate the influence of the grain size distribution after the solidification on the subsequent manufacturing steps, a small scale deformation test was used. A cylindrical sample with a length of 10 mm and diameter of 5 mm was compressed and subsequently heat treated using the quenching and deformation dilatometer DIL805A/D from TA Instruments. The numerical simulation of the deformation and post-heat treatment was set up identically to the experimental testing. An artificial virtual casting of the cylindrical sample was performed before the deformation step. In reality such subsequence of processing steps would correspond to e.g. metal casting with a following hot extrusion process. The

main goal was to demonstrate the influence of a heterogeneous grain size distribution from solidification on the microstructure evolution (static recrystallization) in the solid state during forming and HT.
Fig. 2 shows the experimental (a) and simulation (b) setups. The specimens were compressed directly after a virtual casting step at one mean constant strain rate and a controlled temperature up to an average true strain of 1. Following the compression test, a post-HT process was performed to investigate the influence of the grain structure formation during the solidification on the next processing steps.

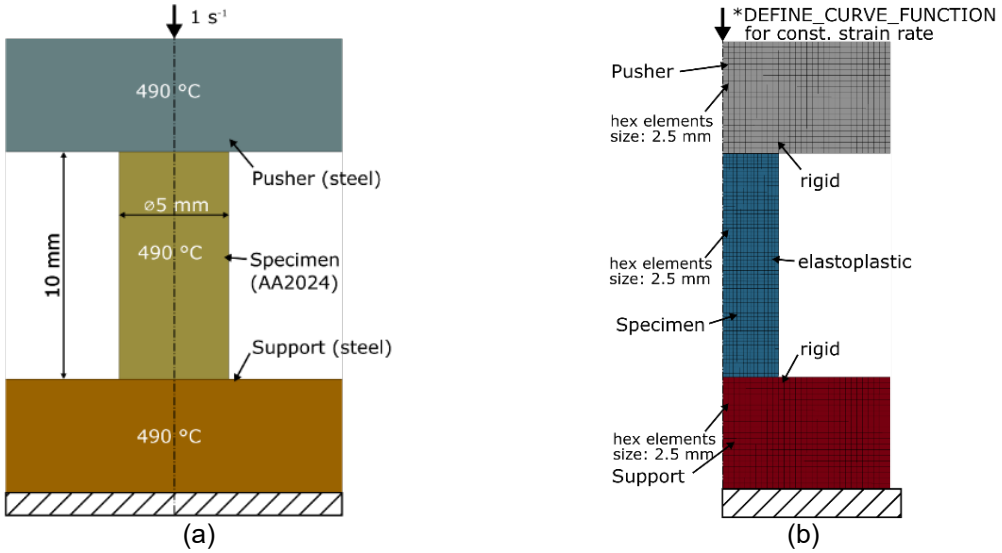

Fig.2: Experimental (a) and numerical (b) setup for the considered compression test.

The most important process parameters for the experimental as well as the numerical compression test are summarized in Tab. 2.

Description	Parameter	Value	Units
Forming temperature	T	490	[°C]
Strain rate	$\dot{\varphi}$	1.0	[s^{-1}]
Post-HT time	t_{dwell}	600	[s]
Post-HT temperature	T_{dwell}	490	[°C]
Initial grain size for homogeneous distribution	d	2.1e-4	[m]

Table 2: Parameters used for the experimental and numerical compression tests.

To obtain the initial microstructure of the compression test sample, the solidification simulation using LB-CA, as described in subsection 2.1, was used. At the start of the grain growth simulation, $T_{init} = T_{liq}$ was set as initial condition. A Dirichlet boundary condition (BC) T_{wall} was defined at all domain boundaries except for the top face side of the billet where a zero gradient BC was applied.
The wall temperature was linearly decreased over time starting from $T_{wall}(t = 0s) = T_0$ until the end of the simulation where $T_{wall}(t = t_{end}) = T_1$. The values prescribed for the boundary conditions are listed alongside the thermal-physical parameters for *AlCu* in Tab. 3.

Description	Parameter	Value	Units
Thermal diffusivity	α	2.38e-5	[m^2s^{-1}]
Liquidus temperature	T_{liq}	917	[K]
Growth kinetics	a_1	8.26e-6	[$ms^{-1}K^{-2}$]
	a_2	8.18e-5	[$ms^{-1}K^{-3}$]
Nucleation law (bulk)	ΔT	5.5	[K]
	ΔT_σ	0.5	[K]
	n_{max}	1e10	[m^{-3}]
Nucleation law (wall)	ΔT	0.5	[K]
	ΔT_σ	0.05	[K]
	n_{max}	1e10	[m^{-3}]

Table 3: Parameters for the grain growth simulation of AlCu alloy.

The growth kinetics parameters were taken from [17]. The domain was discretized using a spatial resolution of $\Delta x = 50\ \mu m$, which is the same order investigated in [17]. The precipitation kinetics was considered using the CALPHAD-based simulation software MatCalc. First, the Scheil-Gulliver simulations were performed and the results (fractions of primary phases) were transferred to the solid-state precipitation (below the solidification temperature). Then, the simulation of the pre-HT (similar to the homogenization step) was performed. Finally, the deformation and post-HT steps were performed with parameters as summarized in Tab. 4.

No.	Process	Temperature [°C]	Heating [min]	Time [min]	Cooling [min]
1	Heating	490	0.5	-	-
2	Forming	490	-	0.017	-
3	Dwell time	490	-	10	-
4	Cooling	20	-	-	-

Table 4: Processing parameters for the deformation and post-HT simulation steps.

All the HT processes were simulated separately using a full 3D bidirectional coupling between LS-DYNA® and MatCalc facilitated by a novel in-house developed clustering technique [18]. The technique was implemented into the flexiCluP (flexible Clustering of Parameters) code to combine elements with sufficiently similar influence parameters for MatCalc (temperature, strain, strain rate) into clusters which trigger only one precipitation kinetics simulation. During coupled simulations, mean cluster values and time step sizes are sent from the MD²M model implemented in LS-DYNA® to a MatCalc session corresponding to the respective cluster and the updated precipitation status such as (N_{part}, r_{part}) is sent back by MatCalc. flexiCluP afterwards redistributes the mean cluster values to the respective elements for further calculations. Thus, the MD²M material model is able to consider solid state precipitations which can affect the recrystallization behavior.

4 Results

In the following, the results from grain growth simulations using LB-CA and the comparison of subsequent compression test results using homogeneous and heterogeneous grain size distribution are presented. The grain growth simulation was performed on a full 3D model LB-CA model with a very fine grid. The mapping and the following forming and HT simulations were performed on a quarter of the 3D geometry where symmetry boundary conditions were utilized. The mapping was used for transferring the data from LB-CA to FEM, as well as to average the grain size information for the much coarser (due to performance limitations) mesh for forming and HT simulations.

4.1 Results from LB-CA calculations

The grain size distribution for the specimen after solidification coming from LB-CA after post-processing is depicted in Fig. 3 (a). During post-processing, the geometrical center point of each grain is calculated and visualized by a sphere of equivalent volume. The whole 3D specimen consists of approximately 200.000 grains with diameters ranging from 62 to 1460 µm. The mean diameter used for the homogeneous case was calculated from the heterogeneous distribution (depicted in Fig. 3 (a)) as 210 µm. Fig. 3 (b) shows the grain size distribution after mapping to a regular FE mesh for LS-DYNA®. Grains are depicted as individual spheres in Fig. 3 (a) where the grain size is equivalent to the sphere diameter and sphere coloring. In Fig. 3 (b), only the coloring matches the average grain size and the spheres correspond to the elements in FEM meshes.

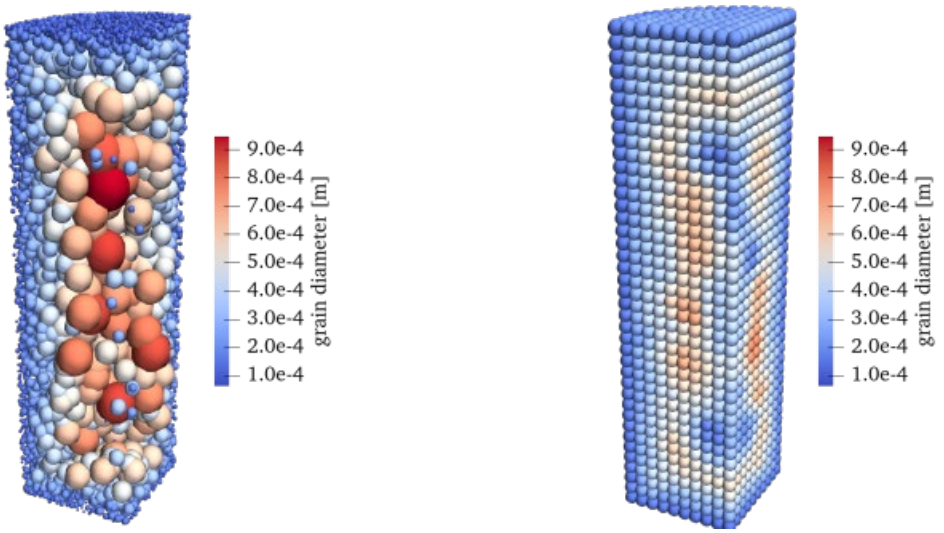

Fig.3: Post-processing of grain size calculated from LB-CA grain growth simulations (a). Grain size results from LB-CA mapped to a regular FEM mesh for LS-DYNA® (b).

Fig. 4 shows the initial grain size distribution for the forming simulation in LS-DYNA® after mapping. Slices are given for 0° (a), 45° (b) and 90° (c).

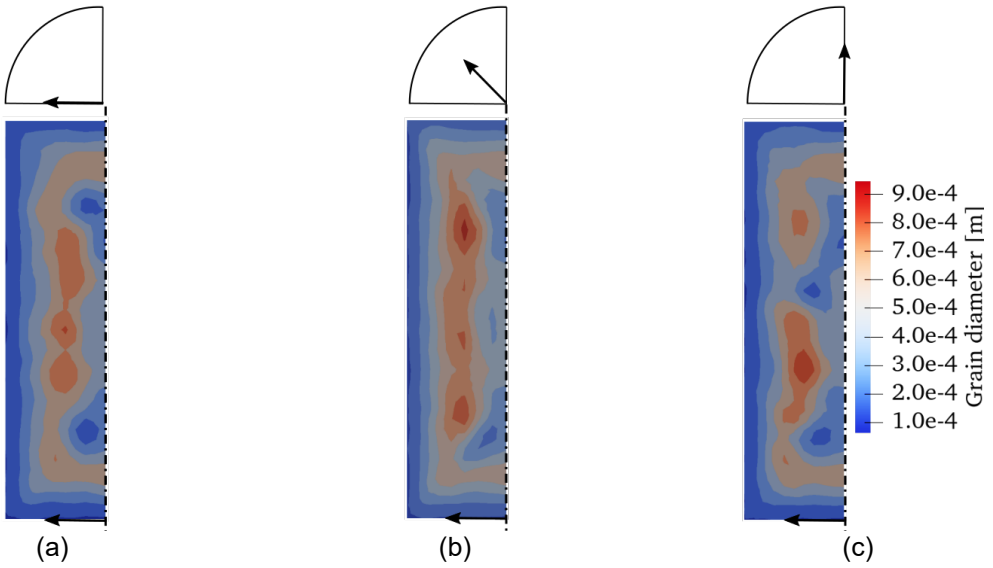

Fig.4: Grain size results for the compression test specimen for three different slices (a-c).

4.2 Results from compression test before post-heat treatment

Two main input variables for the static recrystallization model coming from the forming simulation are final values of dislocation density, ρ, (see Eq. (2)) and sub-grain boundary energy, γ_{sub} (see Eq. (3)). They are used in Eqs. (6-7) for calculating the driving and retarding force of the static recrystallization. The influence of the grain size distribution, d, is currently implemented only for the static recrystallization model during the post-heat treatment step. Therefore, the results from compression test simulations using the heterogeneous and homogeneous grain size distribution are identical in this work. Fig. 5 (a) demonstrates the distribution of dislocation density, ρ, after the deformation. It is mainly influenced by the strain distribution (see Eq. (2)) since the temperature is homogeneously distributed due to the small sample size and the inductive heating system of the DIL805A/D. At the end of the deformation step, the results (final values of ρ and γ_{sub} depicted in Fig. 5) were transferred to the sub-sequent HT simulations. For this, the LS-DYNA® restart methodologies (dynain file) were used. The distribution of subgrain boundary energy is depicted in Fig. 5 (b).

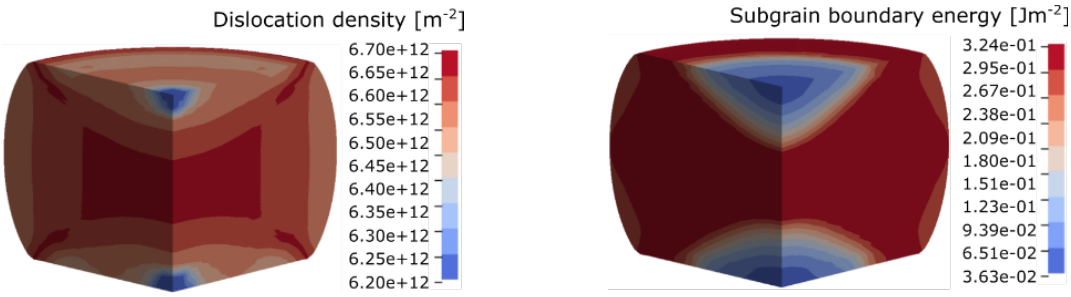

Fig.5: Results from the compression test simulation using MD²M model implemented into LS-DYNA®: dislocation density (a) and sub-grain boundary energy (b) after compression up to strain of 1.

4.3 Comparison of results from heat treatment simulations using homogeneous and heterogeneous grain size distributions

In Fig. 6 and Fig. 7, the final results for the homogeneous (a) and heterogeneous (b) initial grain size distribution for the post-heat treatment after the deformation step, are given. The final recrystallized fraction (Fig. 6) and grain size distribution (Fig. 7) where obtained after post-HT for 600 s.

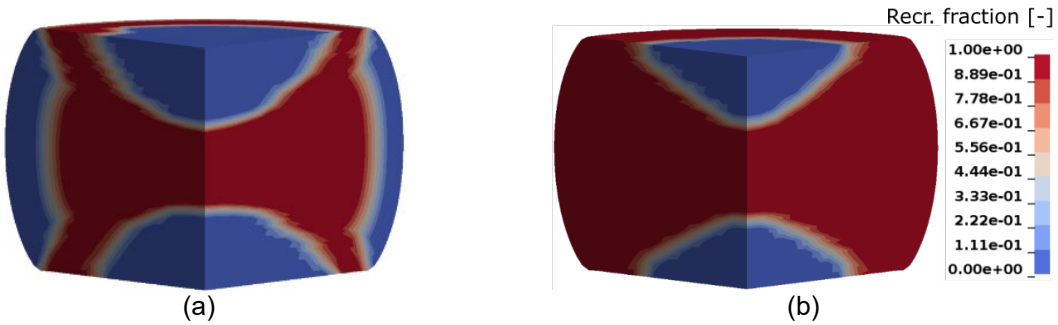

Fig.6: Resulting recrystallized fraction from HT simulations after post-HT for 600 s using the homogeneous (a) and heterogeneous (b) initial grain size distribution.

The influence of the different starting conditions (grain size distribution) can be easily detected in the results. When considering the heterogeneous grain size distribution after the solidification simulation, the recrystallization spreads towards the edges of the sample (see Fig. 6 (b)). This in turn influences the average grain size in the end of the post-HT (Fig. 7 (b)).

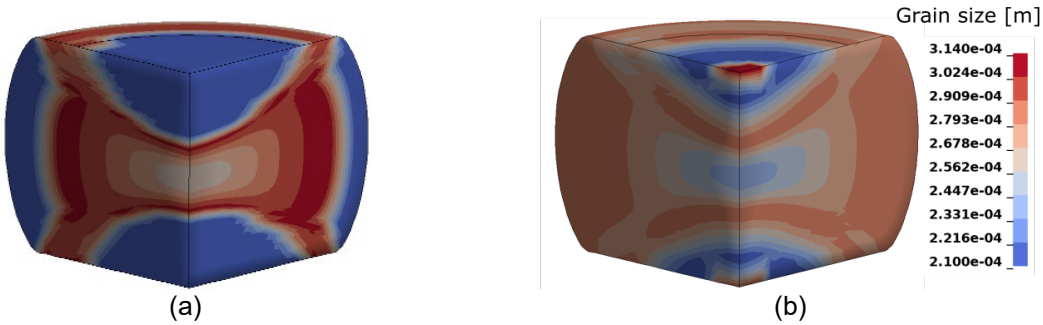

Fig.7: Resulting grain size distribution from HT simulations after post-HT for 600 s using the homogeneous (a) and heterogeneous (b) initial grain size distribution.

Fig. 8 shows the temperature development during HT after solidification (a) and the evolution of grain size (b) at the specimen center for the heterogenous case. Diagrams in Fig. 8 are sliced to better fit and because the missing part is during forming where no additional information from precipitation kinetics is available. Red lines correspond to HT before deformation and blue lines to HT after deformation.

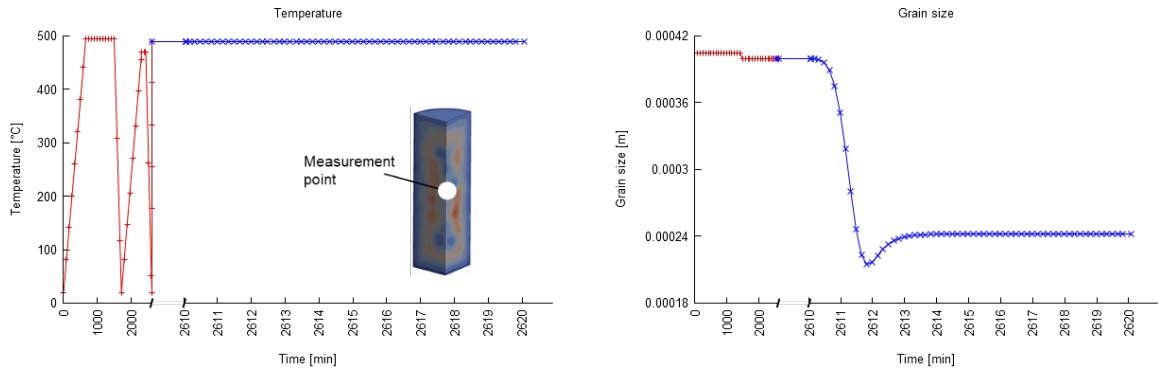

(a) (b)

Fig.8: Results from coupled FEM/precipitation kinetics simulations using predefined temperature (a) obtaining grain size (b).

The average grain size reduces quickly in the beginning of post-HT which correspond to the start of the static recrystallization when new recrystallized nuclei are forming and increases due to the growth of new formed grains.
Fig. 9 shows a micrograph of the cylindrical sample deformed at 490 °C for a strain of 1 after the isothermal post-heat treatment for 600 s. The sample was cut from the large casting billet and thus represents a local microstructure which can be considered homogeneous due to the small sample size. As can be seen, the corresponding simulation results are similar to the measured distribution of the grain sizes and recrystallized fractions for the homogeneous initial grain size distribution (compare Fig. 9 (a) with Fig. 9 (b) and Fig. 6 (a)). This confirms the correct setup of numerical simulations. In the whole casting billet, the distribution of grain sizes after the solidification is, however, heterogeneous and a similar effect on the final microstructure as in Fig. 6 (b) and Fig. 7 (b) can be expected. The demonstration of this effect for simulation of a casting billet of real sizes is part of on-going work and upcoming publications.

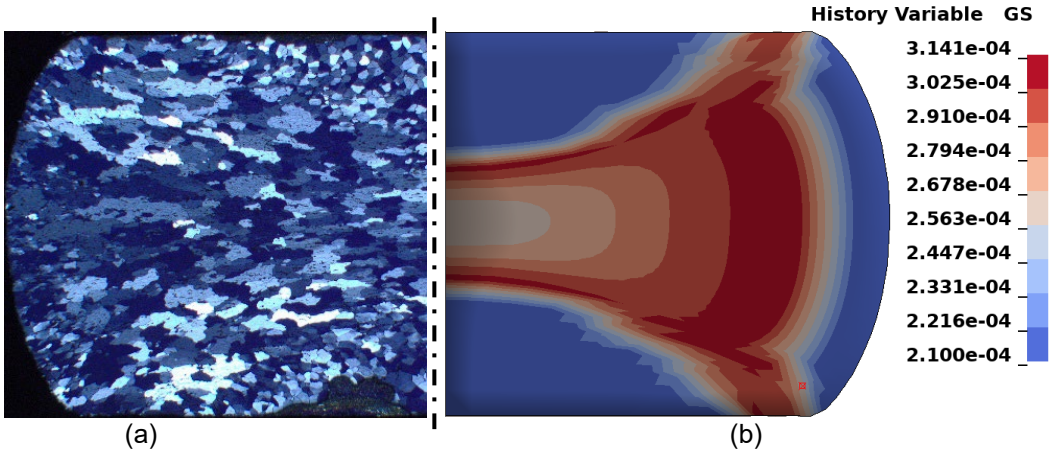

(a) (b)

Fig.9: Micrograph (a) and the corresponding simulation results (b) for grain size from homogeneous initial distribution of the cylindrical sample deformed at 490 °C for a strain of 1 after the isothermal post-heat treatment for 600 s.

5 Summary

In present work, the influence of the initial grain size distribution from solidification simulations (LB-CA model) on the subsequent forming and heat treatment process chain was investigated. Results of the isothermal heat treatment after the deformation using the heterogeneously distributed initial grain sizes in the solidified grain structure showed a significant effect in comparison with results from the initially homogeneous grain size distribution. Especially, the recrystallized fraction and average grain size demonstrated different values depending on the process history. The present work opens the opportunity for further investigations of more complex geometries for industrial applications (e.g. extrusion, rolling etc.).

6 Literature

[1] A. Ockewitz, D. Z. Sun, F. Andrieux and S. Mueller: “Simulation of Hot Extrusion of an Aluminum Alloy with Modeling of Microstructure”, KEM, 491, 2011, pp. 257-264.
[2] P. Sherstnev, C. Melzer and C. Sommitsch: “Prediction of precipitation kinetics during homogenisation and microstructure evolution during and after hot rolling of AA5083”, Int. J. Mech. Sci. 54, 2012, pp. 12-19.
[3] P. Sherstnev, P. Lang, E. Kozeschnik: “Treatment of Simultaneous Deformation and Solid-state Precipitation in Thermo-Kinetic Calculations”, Proc. of 6th Eur. Cong. on Comp. Meth. Appl. Sci. Eng. (Vienna), 2012, p. 4709.
[4] E. Kabliman, P. Sherstnev, J. Kronsteiner, T. Ebner: ”Physikalisch basierte Simulation des Rekristallisationsverhaltens in einer Al-Cu-Mg-Mn Legierung während der Warmumformung und anschließender Wärmebehandlung“, Tagungsband der 8. Ranshofener Leichtmetalltage (Geinberg), 2014, pp. 50-60.
[5] H. J. Bungartz et al.: ”preCICE – A Fully Parallel Library for Multi-Physics-Surface Coupling”, Computers and Fluids 141, 2016, pp. 250-258.
[6] Ch.-A. Gandin, M. Rappaz: “A 3D Cellular Automaton algorithm for the prediction of dendritic grain growth”, Acta mater. 45, 1997, pps. 2187-2195.
[7] J. Latt et al.: “Palabos: Parallel Lattice Boltzmann Solver”, Computers & Mathematics with Applications, 2021, pp. 334-350.
[8] W. Kurz, B. Giovanola, R. Trivedi: “Theory of microstructural development during rapid solidification”, Acta Metallurgica 34(5), 1986, pp. 823-830.
[9] E. Kozeschnik, B. Buchmayr: “MatCalc - A simulation tool for multicomponent thermodynamics, diffusion and phase transformations”, Mathematical Modelling of Weld Phenomena 5, 2001, pp. 349-361.
[10] G.H. Gulliver: “The quantitative effect of rapid cooling upon the constitution of binary alloys”, J. Inst. Met. 47(9), 1913, pp. 120–157.
[11] E. Scheil: “Bemerkungen zur Schichtkristallbildung“, Zeitschrift für Metallkunde 34, 1942, pp. 70–72.
[12] U. F. Kocks: "Laws for Work-Hardening and Low-Temperature Creep.", ASME. *J. Eng. Mater. Technol*. 98(1), 1976, pp. 76–85. https://doi.org/10.1115/1.3443340
[13] H. Mecking, U. F. Kocks: “Kinetics of flow and strain-hardening”, Acta Metallurgica 29(11), 1981, pp. 1865-1875.
[14] E. Kabliman, et al.: “Application of symbolic regression for constitutive modeling of plastic deformation”, Appl. in Eng. Sci. 6, 2021. https://doi.org/10.1016/j.apples.2021.100052
[15] J. Kronsteiner, D. Horwatitsch, I. Baumgartner: ”Impact of temperature rise on deformation dilatometer test method“, SSTT2014, Leibnitz, Austria.
[16] F. Lindner, M. Mehl, B. Uekermann: “RADIAL BASIS FUNCTION INTERPOLATION FOR BLACK-BOX MULTI-PHYSICS SIMULATIONS”, Coupled Problems, 2017, Greece.
[17] Ch.-A. Gandin, M. Rappaz: “A coupled finite element-cellular automaton model for the prediction of dendritic grain structures in solidification processes”, Acta Metallurgica et Materialia 42(7), 1994, pp. 2233-2246.
[18] J. Kronsteiner, E. Kabliman: “Zoning method for efficient material properties calculation”, 15th Int. LS-DYNA® Users Conference, 2018, Detroit, Mi.

Acknowledgements

The authors would like to thank the State of Upper Austria, the BMK and FFG for partial financial support of this research work in the frame of the projects PSHeRo:ER (\#Wi-2020-700757/4-Höf) within the strategic program ‘upperVISION2030’ and within the COMET project AMALFI (872641).